Organic & Biomolecular Chemistry

PAPER

View Article Online
View Journal

Cite this: DOI: 10.1039/c8ob02980f

Glycosylated naphthalimides and naphthalimide Tröger's bases as fluorescent aggregation probes for Con A†

Elena Calatrava-Pérez,[a] Jason M. Delente,[a] Sankarasekaran Shanmugaraju,[a] Chris S. Hawes,[b] Clive D. Williams,[c] Thorfinnur Gunnlaugsson *[a] and Eoin M. Scanlan *[a]

Received 29th November 2018,
Accepted 20th December 2018

DOI: 10.1039/c8ob02980f

rsc.li/obc

Herein we report the synthesis of fluorescent, glycosylated 4-amino-1,8-naphthalimide (**Nap**) **1**, and the related 1,8-naphthalimides Tröger's bases (**TBNap**) **2** and **3**, from 1,8-naphthalic anhydride precursors, the α-mannosides being introduced through the use of CuAAC mediated 'click' chemistry. We investigate the photophysical properties of these probes in buffered solution and demonstrate their ability to function as fluorescent probes for Concanavalin A (Con A) lectin. We show that both the **Nap** and **TBNap** structures self-assemble in solution. The formation of the resulting supramolecular structures is driven by head-to-tail π–π stacking and extended hydrogen bonding interactions of the Nap and the triazole moieties. These interactions give rise to spherical nano-structures (*ca.* 260 nm and 100 nm, for **1** and **3**, respectively), which interact with the Con-A protein, the interaction being probed by using both luminescent and Scanning Electron Microscopy imaging as well as dynamic light scattering measurements. Finally, we show that these supramolecular assembles can be used as luminescent imaging agents, through confocal fluorescence imaging of HeLa cells of the per-acetylated version **2**.

Introduction

The development of small-molecule targeted fluorescent probes and sensors remains an area of intensive research interest,[1–3] particularly for use in live-cell analysis and imaging as high-resolution fluorescence imaging[4,5] techniques have advanced significantly in recent times.[6] Applications of such probes include ion-sensing,[7] subcellular imaging[8] and protein tracking[9] amongst other supramolecular applications.[10] However, significant challenges in the development of such probes arise because many molecular probes/sensors can be cytotoxic, give rise to immunogenic response, and are prone to enzymatic degradation.[11] For real time imaging in cells, insufficient water solubility and lack of targeting ability for specific proteins and enzymes remain a major obstacle.[12,13] We have recently demonstrated the real time monitoring of enzymatic activities in competitive media using enzyme targeting luminescent probes.[11] We have also shown that enzymatic activation (*e.g.* hydrolysis), coupled with the use of fluorescent therapeutics, that have been structurally modified to be selectively recognised by a specific enzyme, can be employed in the generation of so called '*pro-probes*'. These are 'probes' or 'bioconjugates', that only become active *in vivo* upon enzymatic triggered release of the therapeutic cargo; the release/delivery being probed by the emission from the cargo itself within cells.[11,14] Herein, we extend this strategy towards the use of proteins as the targeting carriers;[15] by developing the glycosylated 4-amino-1,8-aphthalimide (**Nap**) **1** and the a 9,18-methano-1,8-naphthalimide-[*b*,*f*][1,5]diazocine ring fused, or Tröger's base based 4-amino-1,8-naphthalimide (**TBNap**) structure **2**, Scheme 1, as fluorescent targeted Concanavalin A (Con A) lectin probes.

Lectins are proteins which specifically recognise and bind to carbohydrates.[16] Lectins are involved in a wide range of biological processes; including regulation of cell adhesion, modulation of protein levels in blood, immune and inflammatory processes, glycoprotein synthesis and the promotion of cell–cell interactions.[17] Lectins have important therapeutic applications in cancer treatment, and are biomarkers for disease and autophagy inducers.[18,19] It is thus not surprising that

[a]*School of Chemistry and Trinity Biomedical Sciences Institute (TBSI), Trinity College Dublin, The University of Dublin, Dublin 2, Ireland. E-mail: gunnlaut@tcd.ie, eoin.scanlan@tcd.ie; http://thorrigunnlaugsson.wordpress.com, http://chemistry.tcd.ie/staff/academic/SCANLAE*

[b]*School of Chemical and Physical Sciences, Keele University, Keele ST5 5BG, UK*

[c]*School of Biochemistry and Immunology and Trinity Biomedical Sciences Institute (TBSI), Trinity College Dublin, The University of Dublin, Dublin 2, Ireland*

†Electronic supplementary information (ESI) available. CCDC 1866499. For ESI and crystallographic data in CIF or other electronic format see DOI: 10.1039/c8ob02980f

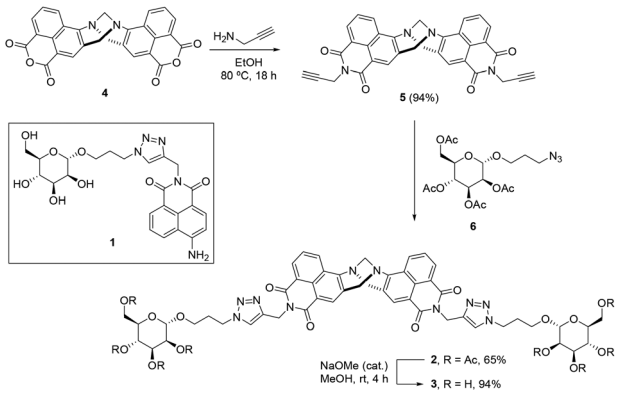

Scheme 1 The structure of **Nap 1**, and the synthetic strategy for the preparation of **TBNap 3** from the **TB** anhydride **4** and the precursor **2**.

lectin recognition is a topical area of research within supramolecular and medicinal chemistry.[17]

Con A is a lectin protein belonging to the legume-type family that preferably binds to α-linked mannosides, but it is also able to bind α-glucosides. With this in mind we designed probe **1**, which consists of a single α-mannoside unit covalently linked to a **Nap**, Scheme 1. Above pH 7, Con A is presented as a tetramer; where each subunit is separated *ca.* 72 Å apart.[20] However, at mildly acidic pH, *e.g.* 4.5–5.5, Con A adopts a di-meric structure. Each monomer contains two metal binding sites for Ca^{2+} and Mn^{2+} ions, which need to be occupied for the sugar binding to take place.[21] In addition to the **Nap** derivative, we developed a divalent system by synthesising the bis α-mannoside **TBNap** derivative **2**, Scheme 1., in order to directly compare the interactions of the mono- *vs.* a divalent probe with Con A. In this article, we present the results from our investigation in the use of **1** and **2** as fluorescent aggregation probes for lectins in solution and compatibility *in vitro* with human cervical cancer cells.

Results and discussion

Design of Nap and TBNap based lectin probes

Using CuAAC chemistry, the **Nap** and **TBNap** probes **1** and **2**, were synthesised as Con A targeted lectin probes; both being synthesised from their corresponding 1,8-naphthalic anhydride structures. **Naps** are well documented fluorophores, possessing internal charge transfer excited state (ICT), that have been extensively used in the development of florescent sensor for ions and molecules, and in medicinal chemistry.[22,23] In contrast to these, the **TBNaps**, are bi-naphthalimide systems, that we have recently developed the application of in significant detail; including their application as anticancer drugs, cellular imaging agents and in MOFs and coordination compounds and polymers, *etc.*[24,25]

Like **Naps**, **TBNaps**, also possess ICT excited state characters, though to lesser extent. Due to the methano-1,5-diazocine ring (N–CH_2–N), the two naphthalimide components of the **TBNaps** units are almost orthogonal to each other, with dihedral angles ranging from 90 to 104°; thus making the **TBNaps** a highly desirable recognition motive for biomolecules.[24,25] With this in mind, both the **Naps** and the **TBNaps** were fully characterised using a range of photophysical techniques, their photophysical as well as their bioavailability properties were investigated.

Synthesis and photophysical analysis of 1–3

Mannosyl-naphthalimide conjugate **1** was prepared according to the reported literature procedures. 4-Nitro-1,8-napthalic anhydride and propargylamine, were first reacted together, followed by conjugation to the per-*O*-acylated mannoside derivative **6** using CuAAC mediated click chemistry under microwave assisted conditions. A reduction of this intermediate, to give the 4-amino analogue, using Pd/C and H_2 at 2 atm., followed by deprotection of the mannose unit, gave **1** in good yield.[11,26] The structure was fully characterised as shown in ESI.†

We have developed many examples **TBNaps** whereby imide end functionalised 3- or the 4-amino-1,8-naphthalimides are reacted with formaldehyde under acidic conditions. This normally results in the formation of the desired **TBNaps**. Unfortunately, this strategy did not work in this case, and the desired compound **3** was difficult to isolate in high purity or yield. Consequently, we moved towards synthesising **3** using an alternative route, based on the use of the TB anhydride **4**, Scheme 1, which was recently developed in our laboratory, and structurally fully charatesised.[27] The anhydride, can be formed in a signal step *via* nucleophilic substitution reaction from a single common 'synthon', a 5-dimethyl-isophthalate based **TBNap** (bis-[*N*-(5-dimethyl-isophthalate)]-9,18-methano-1,8-naphthalimide [*b*,*f*][1,5]diazocine), upon treatment with aqueous KOH. The anhydride was reacted with propargylamine in refluxing ethanol to furnish the dialkyne compound **5** in 94% yield. Compound **5** was then reacted under CuAAC conditions in the presence of per-*O*-acylated mannoside derivative **6**, displaying an alkylazide group at the anomeric position to furnish the protected product **2** in 65% yield. Treatment of **2** under Zemplén conditions furnished the desired product **3** in 98% yield. Both compounds **2** and **3** were characterised (*cf.* Experimental and ESI†) using conventional methods, including both NMR and HRMS. The ^{1}H NMR of **2** (400 MHz, DMSO-d_6) indicated that some aggregation or self-assembly formation occurred in solution, with several broad resonances assigned to the aromatic protons, while the protons assigned to the diazocine moiety appeared as well resolved set of signals between 5.5–5.0 ppm. The HRMS (MALDI) of **1–3** gave the accurate mass for $[M + H]^+$; which in the case of **3**, was found to be m/z = 1063.38054, for $C_{51}H_{55}N_{10}O_{16}$.

Photophysical characterisation of 1–3

Amino-naphthalimides such as **1** have push–pull based intramolecular charge transfer (ICT) based photophysical properties. Their absorption and fluorescence emission spectra are therefore broad and occur within the UV-Vis and the visible regions, possessing moderately large Stokes shift, as

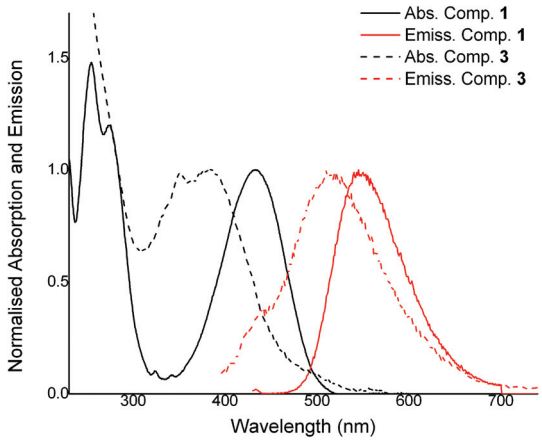

Fig. 1 Normalised absorption and emission spectra for **1** (black solid and black dotted) and **3** (red solid and red dotted).

shown in Fig. 1. Naps also normally possess reasonable lifetimes and quantum yields (Φ_F). The photophysical characterisation of both **1** and **3** was carried in phosphate buffered saline (PBS) solution. Probe **1** displayed an absorption band centred *ca.* 430 nm (ε = 12 300 M^{-1} cm^{-1}) characteristic of the intramolecular charge transfer (ICT) process, and a fluorescence emission with its maximum at 530 nm upon excitation at λ_{max} at 433 nm. The Φ_F was also measured as under these conditions as 11% (see ESI† for details). The fluorescence excitation spectrum mirrored that seen in the absorption spectrum (see ESI†). In the case of **3**, a broad absorption band centred at 380 nm (ε = 9000 M^{-1} cm^{-1}), with a shoulder *ca.* 350 nm was observed. The emission spectra of **3** showed a band centred at 510 nm. Therefore, both the absorption and emission spectra of the **1** are 50 nm blue-shifted with respect to **3**. This blue-shift is due to the substitution of the 4-amino group, reducing the ICT (the push–pull) process. In a similar manner, the per-*O*-acetylated mannose **2**, was also investigated and the UV-Vis absorption and emission spectra matched that observed for **3**.

Self-assembly formation in solution and solid-state analysis of 7

As the **Naps** are known to take part in 'head-to-tail' aggregation through π–π interactions, aggregation studies were undertaken in solution, where both the absorption and the fluorescence emission were monitored for **1** and **3**. It is also well known that sugars and short carbohydrates can self-assemble into higher order structures. These studies were carried out in pH 7.2 DPBS (Dulbecco's phosphate-buffered saline), by varying the concentrations of these two structures between 1×10^{-6} to 1×10^{-4} M. While the absorption spectrum (see ESI†) was not significantly affected, and the Beer–Lambert plot gave a linear slope, the florescence emission of both compounds was significantly affected at concentrations greater than 5×10^{-5} M in the case of **3**. For both systems, the emission was quenched at elevated concentrations, Fig. 2.

In the case of **3**, no significant changes were observed in the λ_{max}, but for the **TBNap 1**, the aggregation seem to be

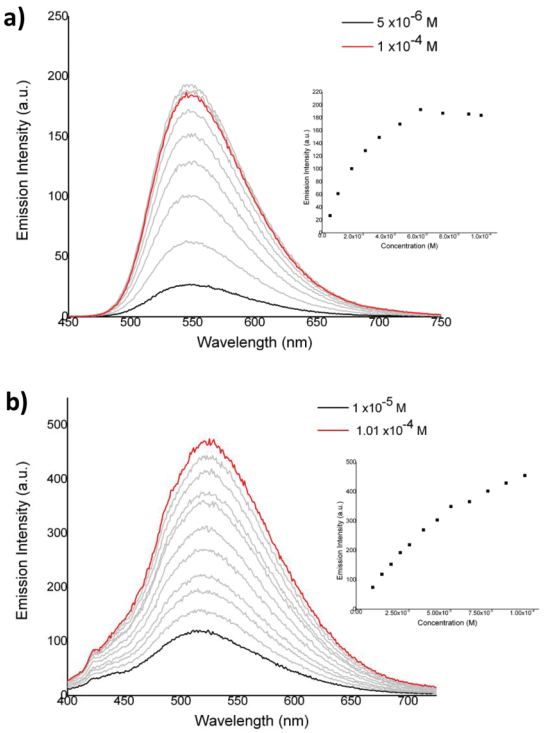

Fig. 2 Changes in the fluorescence emission of (a) **1** and (b) **3** in DPBS at room temperature upon changing the concentrations of these two structures between 1×10^{-6} to 1×10^{-4} M. Inset: The changes in the emission intensity at λ_{max} as a function of increasing concentration of **1** and **3**, respectively.

occurring at slower rate, while being concomitantly causing blue shift in the λ_{max}. The quenching is characteristic of naphthalimides π–π stacking interactions, in addition to hydrogen bonding interactions between the imide and the 4-amino moieties of stacked **Naps** 'dimers'.[23c] These interactions giving rise the formation of columns of such stacked structures, which are often stabilised by solvent interactions, such as hydrogen bonding to interstitial water protons. In the case of **1** and **3**, we anticipated that these supramolecular interactions would be further aided by the mannoside moieties, which would be expected to take part in the formation of higher order self-assembly formations, through extended and multiple intermolecular hydrogen bonding interactions.

We have in the past characterised such 'head-to-tail' interactions both in solution as well as in the solid-state; these normally showing a clear hydrogen bonding interaction between the amino group of the **Nap** moiety.[23c] However, attempts to crystallise either **1** or **3** on all occasions did not result in the formations of crystals suitable for solid state crystallographic analysis. We were however, able to obtain crystals of the **Nap** structure **7**, Fig. 3, which is structurally related to **1**, with the exception that the mannoside moiety is missing. This 'model' compound was previously synthesised in our laboratory by subjecting a glycosylated **Nap** 'pro-probe' to the glycosidase enzymes β-galactosidase, which rapidly hydrolysed the glycosidic bond, concomitantly releasing **7** into cancer cells.[11] **7**, and

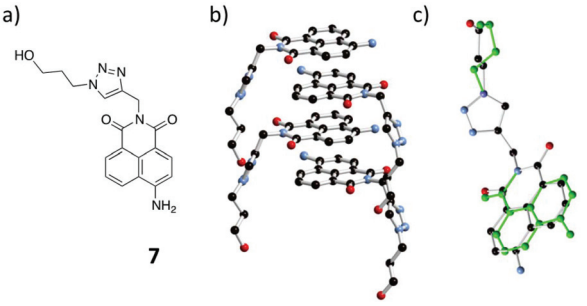

Fig. 3 (a) Chemical structure of compound **7**. (b) The X-ray crystal structure formed in H_2O, and the extended π–π interactions, and (c) the two disordered orientations of the naphthalimide and alcohol fragments (minor conformer shown in green).

is a good model of **1**, as it allows us gain inside into the various supramolecular interactions occurring at the **Nap** and the triazole moieties.

The structure of **7** is shown in Fig. 3a, as well as the packing in the solid state in Fig. 3b.[33] As can be seen in Fig. 3b, the **Naps** display π–π stacking interactions, being arranged with a near-120° rotation between the major axes of each successive **Nap**. This orientation is different to what we have observed before, where a true head-to-tail orientation is typically observed. These interactions give rise to stacked columns; the chains are bent to shroud the exterior of the columns and engage in hydrogen bonding interactions with neighbouring groups.

There are three types of hydrogen bond donor in the compound: the amine and alcohol groups and the triazole C–H group. The alcohol and imide oxygen atoms and one triazole nitrogen atom act as hydrogen bond acceptors. The **Nap** molecules interact further with a molecule of water, shared between four **Nap** molecules, forming hydrogen-bonding interactions with the terminal alcohol. One could envisage that such interactions could be potentially greater for **1** and **3**, given the number of additional hydrogen bonding acceptors/donors available. As the more directional interactions take place at the peripheries of the molecule, substantial crystallographic disorder is observed on the core atoms. This is related to the tendency of the central **Naps** to orient across two positions related by rotation (Fig. 3c), with a distribution 2 : 1 or 1 : 1 for the two unique residues. It is clear from these results that the **Nap** structures can partake in self-assembly processes, that could result in the formation of higher-order materials, and that this could potentially affect their biological applications. As **1** and **3** were developed as fluorescent probes for Lectin protein, we set out to investigate both the affinity of this binding interaction, through the use of fluorescent titrations, as well as how this would affect the 'material' nature of **1** and **3** using Scanning Electron Microscopy (SEM) imaging.

Con A binding studies

In order to investigate if the **Nap** compounds could function as molecular probes for lectin proteins, we evaluated the changes in their luminescent properties upon addition of Con A to solutions of **1** and **3**. Based on our investigation above, we postulated that following addition of Con A, the carbohydrate–lectin binding interactions would occur and potentially disrupt aggregates resulting in significant changes in the fluorescence. As a qualitative test, 0.1 equivalents of Con A were initially added to a 1×10^{-4} M solution of **1** and **3**, respectively, Fig. 4a and b, in pH 7.2 DPBS solution, in the presence of 0.1 mM $MnCl_2$ and 0.1 mM $CaCl_2$ at 25 °C. In the case of **1**, the fluorescence was enhanced significantly upon the addition of Con A, highlighting its ability to interact with Con A, and function as a lectin probe.

In contrast to this, the fluorescence intensity for **3** decreased at λ_{em} = 510 nm but a new shoulder appeared at 450 nm. This could possibly be due to the presence of the Tröger's base moiety, which places the two **Naps** part almost orthogonal. We have observed similar effect upon binding Ru(II) polypyridyl based **TBNap** upon binding to DNA.[25] Similarly, we analysed the binding of **2** to Con A. However, no changes were observed in the fluorescence emission, indicating that acetylated version was unable to bind to the protein in the same manner as **3** (see ESI†). Having established that both compounds **1** and **3**, interacted with Con A, a titration of **1** and **3** (1×10^{-4} M) with Con A was undertaken (using final concentrations of Con A between 10^{-6} and 10^{-4} M). Here, significant changes were observed in the emission of **1**, which was enhanced. The changes in the ICT band at 535 nm are shown in Fig. 4c as a function of emission enhancement $(F - F_0)$ where it is clear that the most significant changes occur at low concentrations of Con A; the emission showing a linear trend upon addition of Con A, until 9×10^{-5} M, after which a saturation point is reached. In a similar manner, the changes in the emission of **3** was monitored. While no significant changes were observed in the λ_{max} at 510 nm, changes were observed at 450 nm shoulder, which also demonstrated a linear enhance-

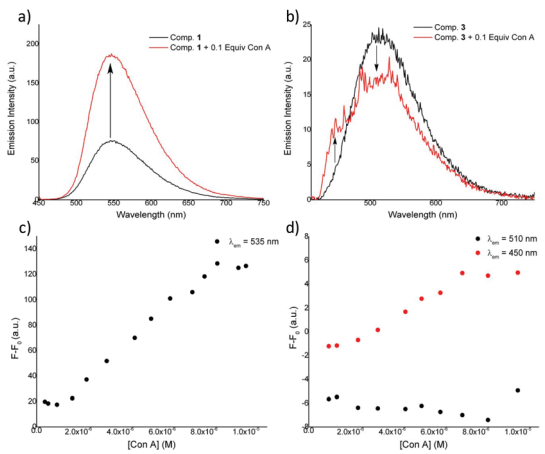

Fig. 4 Changes in the fluorescence emission intensity of **1** (a and c) and **3** (b and d), respectively, upon addition of 0.1 equiv. of Con A and varying concentrations of Con A. In pH 7.2 DPBS solution, in the presence of 0.1 mM $MnCl_2$ and 0.1 mM $CaCl_2$ at 25 °C.

ment occurred within the same concentration window as that seen for **1**, namely, between 2×10^{-6} and 8×10^{-5} M of Con A. The titrations also showed that below 1 μM Con A concentration, no changes were observed, Fig. 4c and d. Unfortunately, we were unable to accurately determine the binding affinity for these interactions.

Binding selectivity

Encouraged by the positive results obtained with **1**, we set out to investigate the effect of the Con A binding under varying conditions, and the results are summarised in Fig. 5. As can be seen in Fig. 5, the addition of Con A (0.1 equivalents) led to a *ca.* 70% increase in the fluorescent intensity of **1**. The addition of two-fold excess of α-D-mannose (compare to Con A) did not affect the emission properties. This could indicate that the probe was fully bound at this concentration. Similarly, no further quenching was observed for **3** upon addition of α-D-mannose at this concentration. In a separate experiment, the probes were incubated with de-natured Con A (heated at 80 °C for 30 min), and no relevant changes in the fluorescent emission were observed, demonstrating that only a specific binding interaction between Con A and the two probes induces a change in the luminescence.

To further validate the binding interactions, the probes were treated with 0.1 equiv. of Bovine Serum Albumin (BSA). Albumin is a prevalent macromolecular transporter protein found in the blood stream due to its capacity to bind and carry small molecules. Significantly, no changes were observed in the luminescence of **1** and **3** in the presence of BSA, demonstrating that the fluorescence changes observed are exclusively due to the selective binding with Con A. Following this experiment, Con A (0.1 equiv.) was added to this mixture to investigate if the presence of BSA would interfere with binding seen above. Gratifyingly, the fluorescence changes followed the same trend as the experiment conducted in the absence of BSA, highlighting that lectin–carbohydrate binding remains efficient in the presence of other macromolecules. This is an important finding in view of these compounds having application as molecular probes *in vitro*.

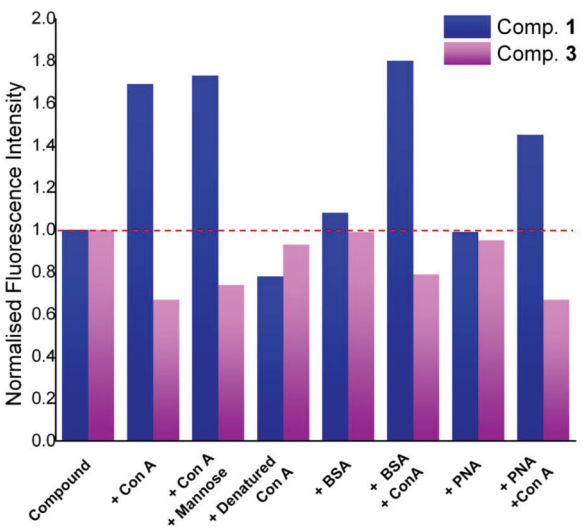

Fig. 5 Normalised fluorescence intensity of **1** (blue) and **3** (magenta) in the presence of different biomolecules, in pH 7.2 DPBS solution, in the presence of 0.1 mM $MnCl_2$ and 0.1 mM $CaCl_2$ at 25 °C.

We repeated this experiment using another relevant lectin Peanut Agglutinin (PNA) which preferably binds to β-Gal-(1–3)-β-GalNAc units, and identical, non-bonding, behaviour was observed for both **1** and **3**. Therefore the changes in the luminescence are clearly only due to the selective binding between the α-mannosides probes and Con A. Finally, as a negative control, two structurally related **Naps**, that have previously developed in our laboratory,[11] possessing a β-galactoside (**Gal-Nap**) and β-Lactoside (**Lac-Nap**) moiety instead of the mannose site employed here, as well as **2**, were treated with Con A (0.1 equiv.) under identical conditions as described above. Importantly, only negligible changes were observed in the fluorescence intensity of all of these probes (see ESI†) upon addition of Con A. We believe that this demonstrates that the aggregation of **1** and **3** is significantly affected upon binding to Con A. As we were unable to accurately determining the binding constants for the interaction of **1** and **3** for Con A, we set out to probe if the nanostructure (*e.g.* the morphology of self-assembly structure of **1** and **3**) would be affected upon binding to Con A. This elucidation was carried out by using SEM imaging.

Morphology studies

The self-assembly or aggregation of **1** and **3** was observed above in solution. To investigate further the material nature of these assembles, pH 7.2 DPBS solution of **1** and **3** were drop casted onto silicon wafer, dried in air and imaged using SEM. The results are shown in Fig. 6 (see also ESI†). From this imaging, it is clear that both **1** and **3** form particles; these being of *ca.* 260 nm and 100 nm average size, Fig. 6a and b, for **1** and **3** respectively (it is also possible to see some salt formation, due to the buffer from which these were casted from). These images further support out findings above that both the **Nap** and the **TBNaps** form self-assembly structures in solutions. The changes in the morphology of both of our probes when interacting with Con A, was next carried out. The SEM images of these are shown in Fig. 6c and d; the samples being formed in identical manner except in the presence of 0.2 equivalents of Con A, and 0.1 mM $MnCl_2$ and 0.1 mM $CaCl_2$, followed by drop casting and drying in air. It is clear form Fig. 6c and d, that the presence of the Con A. and the salts has significant effect on the morphology of both **1** and **3**. While some indications of the presence of the nanospheres can be seen for **1**, it is clear that significant aggregation has occurred in the present of the protein, and as above, in the presence of salts. However, SEM imaging of the protein itself (drop casted from buffered ionic solutions), demonstrated the formation of thick films which lack the morphology seen in Fig. 6c (see ESI†).

Similarly, the morphology of the **TBNap 3** in the present of Con A is significantly different to the self-assembly of **3** alone;

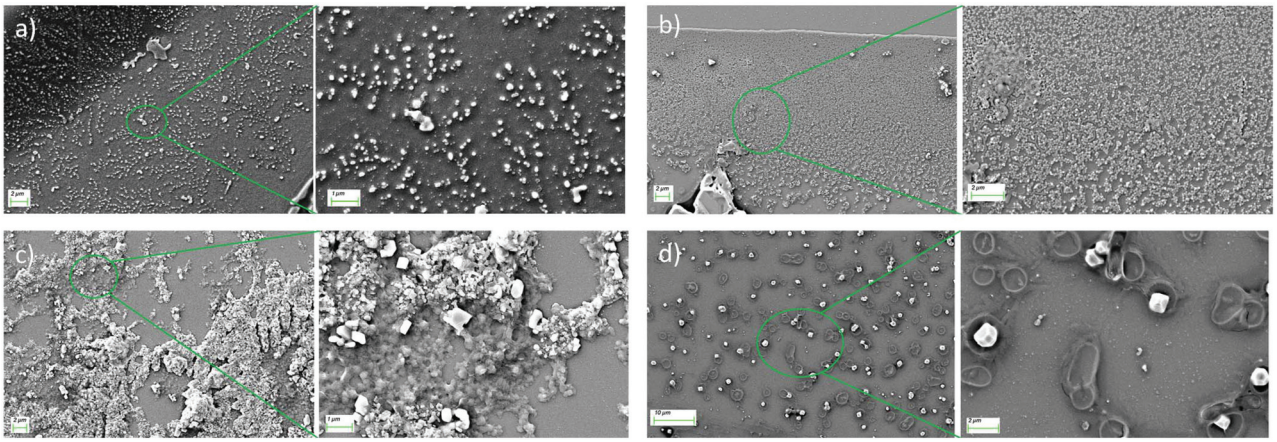

Fig. 6 SEM images of **1** before (a) and after addition of 0.1 equiv. of Con A (c) and **3** before (b) and after addition of 0.1 equiv. of Con A (d), showing significant morphological changes that demonstrate the binding with Con A, after drop-casting from buffered pH 7.2 solutions of these compounds. The formation of salts is also visible in these images.

the presence of larger aggregates is observed that seem to consist of spherical structures, some of which seem to indicate a 'collapsed' hallow-spheres. These results provided further evidence that these structures do interact with Con A resulting in changes in their morphological features. To probe if the DPBS buffer had an effect on the morphology of both probes, the samples were prepared in pure deionised water, and the resulting solution of **1** and **3** drop casted onto silicon wafer, dried in air followed by few hours under vacuum and imaged using SEM (see ESI†). Gratifyingly, the two samples showed similar morphology to that seen for samples prepared in DPBS demonstrating that the buffer did not influence the morphology of both probes and that the changes observed previously are due to the presence of Con A. This observation was also supported by DLS measurement that were carried out on **3** in both the absence and presence of **Con A** in DPBS buffer. Here, the DLS showed that the average size of the aggregates in solution for the **3** alone was similar to that seen in the SEM, while these were almost ten times the size upon interacting with Con A (see ESI†).

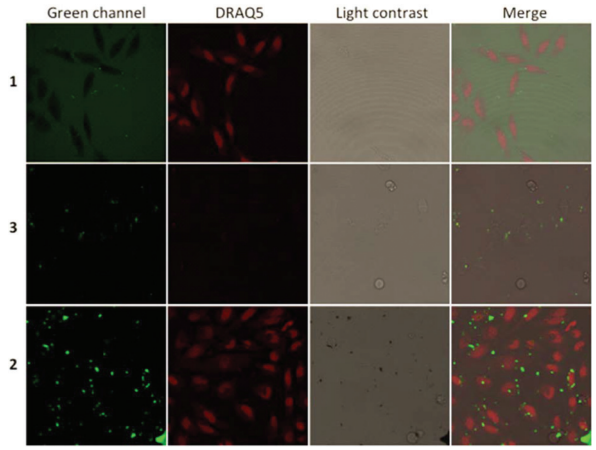

Fig. 7 Confocal images of HeLa cells treated with compound 1 (50 μM, first row), compound **3** (50 μM, second row) and compound **2** (50 μM, third row) after 24 h incubations. Compounds were excited by a 405 nm argon laser, emission 450–550 nm, DRAQ5 was excited by a 633 nm red helium–neon laser, emission >650 nm. *Compound **3** was not incubated with DRAQ5 as it quenched its fluorescence emission.

Biological evaluation

Having demonstrated that **1** and **3** could interact with lectin proteins, and that no interaction was seen with proteins such as BSA (Fig. 5), we investigated the biological scope of **1–3** *in vitro* using human cervical cancer cells (HeLa). We have previously performed uptake studies of **1** across various cell lines where no uptake was observed, even after long incubation times (24 h) (Fig. 7, first row). However, **3** was shown to localize within the cytosol of the HeLa cells (Fig. 7, second row) within 24 h; possibly due to the greater lipophilicity of **3** *vs.* **1**. However, compound **3** was not shown to be toxic, with IC_{50} values >100 μM (evaluated *via* Alamar Blue assay). Longer incubation times (72 h), also resulted in IC_{50} that were greater than 100 μM, therefore it can be concluded that **3** could be used safely *in vitro*. To support this rationale, compound **2** was also evaluated *in vitro*, as the protected mannose units make it even more lipophilic and therefore more prone to cellular uptake. Incubation in HeLa cells (Fig. 7, third row) showed a greater uptake than either **1** or **3**. However, due to its high hydrophobicity it was observed to form aggregates in aqueous solution. Interestingly, short times of incubation (of *ca.* 1 h) showed larger aggregates that are more challenging for cellular uptake, and these aggregates interact with the cell membrane (see ESI†). After longer times (24 h), the aggregates reduce in size and are increasingly accumulated within the cells. Confocal imaging analysis through the use of *Z*-stacks images proved that the smaller aggregates were indeed located inside the cells whereas the larger ones only interact with the cell membrane (see ESI†).

Conclusions

Two structurally related glyconaphthalimide probes were prepared and their photophysical and self-assembly properties investigated. Their ability to function as fluorogenic molecular probes for lectin binding was studied and it was demonstrated that carbohydrate–lectin interactions resulted in a disruption of aggregation that resulted in significant changes in fluorescence. Binding studies in the presence of non-lectin proteins demonstrated that changes in the luminescence arise from selective binding interactions between the α-mannosides probes and Con A and highlight the potential of these probes for *in vitro* and *in vivo* applications. The monovalent **1** probe was found to be superior to **3** for lectin detection although **3** more readily underwent cellular uptake in HeLa cells. Detailed morphology studies further confirmed the disruption of aggregates upon carbohydrate–lectin binding interactions. This proof of principle opens novel avenues for molecular probe design using naphthalimide derivatives. We are currently investigating the use of **TBNap** structures as supramolecular synthons for the formation of self-assemble in solutions for applications in chemical biology.

Experimental

Materials and methods

Unless otherwise stated; all commercial chemicals were obtained from Sigma-Aldrich or Fluka and used without further purification. Deuterated solvents for NMR use were purchased from Apollo. Dry solvents were distilled under Argon and dried over 4 Å molecular sieves prior to use. Solvents for synthesis purposes were used at GPR grade. NMR spectra were recorded on Bruker DPX-400 Advance spectrometers, operating at 400.13 MHz and 600.1 MHz for ^{1}H NMR; 100.6 MHz and 150.9 MHz for ^{13}C-NMR. Shifts are referenced to the internal solvent signals.[1] NMR data were processed using Mestrenova software. HRMS spectra were measured on a Micromass LCT electrospray TOF instrument with a WATERS 2690 autosampler and methanol/acetonitrile as carrier solvent. Melting points were determined using a Stuart Scientific Melting point was determined using an Electrochemical IA9000 digital melting point apparatus in an unsealed capillary tube and are incorrect. Infrared spectra were recorded on a PerkinElmer Spectrum One FT-IR Spectrometer equipped with a Universal ATR sampling accessory. Carbohydrate positions are named 1 to 6, starting the count in the anomeric position.

UV/Vis measurements

UV-visible absorption spectra and optical density were recorded by means of a Varian CARY 50 spectrophotometer. Solutions were measured in 3 cm (10 mm × 10 mm) cuvettes. The wavelength range was 200–600 nm with a scan rate of 300 nm min^{-1}. The solvents employed were HPLC or spectrophotometric grade.

Fluorescence measurements

Fluorescence measurements were made with a Varian Carey Eclipse Fluorimeter equipped with a 1.0 cm path length quartz cell. The solvents used were of HPLC grade. The concentrations of the compounds under investigation were the same as those used for the UV-visible absorption measurements.

Cell culture

HeLa cells were grown in Dulbecco's Modified Eagle Medium (Glutamax) supplemented with 10% fetal bovine serum, 1% penicillin/streptomycin and 0.2% of plasmocin at 37 °C in a humidified atmosphere of 5% CO_2.

Alamar blue viability assay

HeLa cells were seeded at a density of 2.5×10^4 cells per well in 96-well plates and treated with the indicated compounds for 24 or 72 h. Alamar blue (22 μl) was then added to each well and incubated at 37 °C in the dark for 4 h. Plates were then read on a fluorescence plate reader (SpectraMax Gemini, Molecular Devices) with excitement and emission wavelengths of 544 nm and 590 nm, respectively. Experiments were performed in triplicate on three independent days with activity expressed as percentage cell viability compared to vehicle treated controls. All data points (expressed as means ± S.E.M.) were analysed using GRAPHPAD Prism (Graphpad software Inc., San Diego, CA).

Confocal microscopy

Cells were seeded at a density of 5×10^4 cells per dish in glass bottom wells and leave to grow for 24 h. Before treatment cell media was replaced by phenol-red free media and cells were incubated with compounds (50 μM) for 1 and 24 h, respectively. Cells were stained with DRAQ5 (red nuclear stain), followed by viewing using Leica SP8 STED confocal microscopy with a 40× oil immersion lens. Image analysis was performed using Leica Application Suite software. Compounds were excited by a 405 nm argon laser, emission 450–550 nm, DRAQ5 was excited by a 633 nm red helium–neon laser, emission >650 nm. Images are representative of three independent experiments.

Scanning electron microscopy

The morphology of the samples were studied using a Carl Zeiss Ultra SEM with an SE2 or in-lens detector in the Advanced Microscopy Laboratory, CRANN, Trinity College Dublin, with the samples deposited on silicon wafers with a thick silicon dioxide layer. Prior to imaging, all samples were coated with a conductive layer of Pd/Au using a Cressington 208Hr high-resolution sputter coater.

X-ray crystallography

The diffraction data were collected on a Bruker APEX-II Duo dual-source instrument using microfocus Cu-Kα radiation (λ = 1.5405 Å) using ω and φ scans. A single crystal was mounted on Mitegen micromounts in NVH immersion oil, and maintained at a temperature of 100 K using a Cobra cryostream.

The diffraction data were reduced and processed using the Bruker APEX suite of programs.[28] Multi-scan absorption corrections were applied using SADABS.[29] The data were solved using the Intrinsic Phasing routine in SHELXT. Although the chiral space group $P2_12_12$ gave the best statistics and most appropriate structure model, no chirality information is assumed and the structure was refined as a racemic twin with full-matrix least squares procedures using SHELXL-2015 within the OLEX-2 GUI.[30–32] All non-hydrogen atoms were refined with anisotropic displacement parameters. All hydrogen atoms were placed in calculated positions and refined with a riding model, with isotropic displacement parameters equal to either 1.2 or 1.5 times the isotropic equivalent of their carrier atoms. Due to the severe disorder in the naphthalimide fragments of both unique molecules, DFIX, SADI and RIGU restraints and EADP constraints were necessary to maintain reasonable chemical geometries and U_{ij} tensors, particularly where atoms from both fragments were closely overlapping. Occupancies of the individual conformers were determined with free variable refinement and then fixed to sensible fractional values. Specific collection and refinement strategies are further outlined in the combined crystallographic information file (cif) under the _refine_special_details heading. CCDC 1866499.†

Crystal data for compound 7 ($C_{36}H_{35}N_{10}O_{6.5}$, M = 711.74 g mol^{-1}): orthorhombic, space group $P2_12_12$ (no. 18), a = 17.0714(12) Å, b = 27.849(2) Å, c = 6.8249(3) Å, V = 3244.7(4) Å^3, Z = 4, T = 100.0 K, μ(CuKα) = 0.859 mm^{-1}, D_{calc} = 1.457 g cm^{-3}, 21 933 reflections measured (6.072° ≤ 2Θ ≤ 137.048°), 5941 unique (R_{int} = 0.0536, R_{sigma} = 0.0544) which were used in all calculations. The final R_1 was 0.0754 ($I > 2\sigma(I)$) and wR_2 was 0.2039 (all data).

Synthetic procedures

Bis-(*N*-(1-(3-(2′,3′,4′,6′-tetra-*O*-acetyl-α-D-mannopyranosyloxy)propyl)-1*H*-1″,2″,3″-triazol-4″-yl)methyl)-9,18-methano-1,8-naphthalimide-[*b*,*f*][1,5]diazocine (2). Compound **5** (28 mg, 0.05 mmol, 1 equiv.), compound **1** (45 mg, 0.1 mmol, 2 equiv.) and Cu(BF$_4$)(MeCN)$_4$ (10 mg, 0.03 mmol, 0.3 equiv.) were dissolved in DMF (5 mL) in a microwave vial. The reaction mixture was stirred for 2 h at 115 °C in a microwave reactor. The solvent was removed *in vacuo* and the crude product dissolved in a mixture of MeOH/CH_2Cl_2 (1 : 2) and filtered through a plug of Celite® to remove the copper catalyst. The filtrate was concentrated *in vacuo* and purified by SiO_2 column chromatography. The product was obtained as an orange wax (40 mg, 66%). **^{1}H** (799.7 MHz, $CDCl_3$): 8.69 (bs, 2H, H–Ar), 8.62 (d, J = 11.4 Hz, 2H, H–Ar), 8.13 (s, 2H, H–Ar), 8.03 (s, 2H, H–Ar), 7.86 (s, 2H, H–Ar), 7.61 (s, 2H), 5.42 (bs, 3H), 5.27–5.24 (m, 4H, CH_2), 5.21 (bs, 1H), 5.14 (app t, 2H, N–CH_2), 4.76 (s, 2H, H-1), 4.66–4.64 (m, 2H), 4.61–4.56 (m, 2H), 4.43–4.39 (m, 2H), 4.38–4.34 (m, 2H), 4.20–4.35 (m, 2H), 4.05 (d, J = 12.6 Hz, 2H), 3.96–3.92 (s, 2H), 3.71–3.67 (s, 2H), 3.40–3.35 (s, 2H), 2.14, 2.06, 2.05, 1.99 (s, 24H, $OCOCH_3$), (2 × CH_2 buried under $OCOCH_3$). **^{13}C** (201.1 MHz, $CDCl_3$): 153.6, 133.5 (C–Ar), 129.8 (C–Ar), 100.4 (C-1), 71.9, 71.6 (C–CH_2), 71.3, 69.6, 68.5 (C–CH_2), 67.3, 67.2, 65.0, 59.7 (C-16), 59.6, 39.2, 37.8, 34.1, 33.7, 33.6, 23.6, 23.5, 23.4, 23.3, 22.4 (7C, $OCOCH_3$). ν_{max} (ATR)/cm^{-1}: 789, 1051 (C–N), 1229 (C–N), 1373, 1597 (ar. C–C), 1659 (C═O), 1747, 2923. **HRMS** (*m*/*z* – MALDI): found: 1421.4504, ([M + Na]$^+$. $C_{67}H_{70}N_{10}O_{24}Na$, required: 1421.4462).

Bis-(*N*-(1-(3-(α-D-mannopyranosyloxy)propyl)-1*H*-1′,2′,3′-triazol-4′-yl)methyl)-9,18-methano-1,8-naphthalimide-[*b*,*f*][1,5]diazocine (3). Compound **2** (40 mg, 0.028 mmol, 1 equiv.) was dissolved in MeOH/NaOMe (5 mL, 0.4 equiv.). After stirring for 4 h at rt, DOWEX® 50WX8-200 ion exchange resin was added to the mixture until a neutral pH was measured. The reaction mixture was filtered and the filtrate concentrated *in vacuo*. Yielding the desired product as an orange powder (28 mg, 98%). **M.p:** 120.5–122.0 °C (decomposition). **^{1}H** (400 MHz, d-TFA): 9.05 (d, J = 8.0 Hz, 2H, H–Ar), 8.99 (d, J = 7.2 Hz, 2H, H–Ar), 8.84 (s, 2H, H–Ar), 8.65–8.59 (m, 2H, H–Ar), 8.36 (s, 2H, H–Ar), 5.96 (s, 2H, H–Ar), 5.93–5.87 (m, 4H, CH_2, H–Ar), 5.83 (s, 2H, N–CH_2), 5.32–5.29 (m, 2H), 5.28–5.25 (m, 2H), 5.22 (s, 2H), 5.00–4.94 (s, 6H), 4.55–4.39 (m, 2H), 4.55–4.29 (m, 2H), 4.19–4.08 (m, 4H), 3.81–3.75 (m, 2H). ν_{max} (ATR)/cm^{-1}: 980, 1100, 1490 (ar. C–C), 1750 (C═O), 3410 (OH/NH_2). **HRMS** (*m*/*z* – ESI): found: 1063.38054, ([M + H]$^+$. $C_{51}H_{55}N_{10}O_{16}$, required: 1063.3792).

Bis-[*N*-(1-propargyl)]-9,18-methano-1,8-naphthalimide-[*b*,*f*][1,5]diazocine (5). Compound **4** (100 mg, 0.21 mmol, 1 equiv.) was reacted with propargylamine (35 μL, 0.54 mmol, 2.5 equiv.) in EtOH (10 mL) at 80 °C for 16 h. After this time, the reaction mixture was filtered through Celite and washed with cold EtOH leaving an orange solid (108 mg, 94%). **M.p:** 292–294 °C (decomposition). **^{1}H** (400 MHz, $CDCl_3$): 8.72 (d, J = 8.4 Hz, 2H, H–Ar), 8.65 (d, J = 7.2 Hz, 2H, H–Ar), 8.14 (s, 2H, H–Ar), 7.88 (app t, 2H, H–Ar), 5.15 (d, J = 16.9 Hz, 1H, N–CH_2), 4.88 (s, 4H, H-2), 4.68 (s, 2H, N–CH_2–N), 4.59 (d, J = 16.9 Hz, 2H, N–CH_2). **^{13}C** (100 MHz, CDCl3): 163.2, 162.6, 150.0, 131.6, 131.1, 131.0, 127.9, 127.78, 127.4, 126.9, 122.5, 117.8, 79.8, 73.4, 66.4, 56.5, 31.2, 29.4, 19.0. ν_{max} (ATR)/cm^{-1}: 1033, 1661 (C═O), 1340 (ar. C–C), 2935 (CCH). **HRMS** (*m*/*z* – MALDI): found: 537.1578, ([M + Na]$^+$. $C_{33}H_{54}N_{10}O_{16}Na$, required: 537.15557).

Conflicts of interest

There are no conflicts to declare.

Acknowledgements

We thank the Irish Research Council (IRC) (GOIPD/2013/442 to S. S., and GOIPD/2015/446 to C. S. H.) and Science Foundation Ireland (SFI PI Award 13/IA/1865 to T. G.) and (SFI CDA Award 15/CDA/3310 to E. M. S.) for the financial support.

Notes and references

1 (*a*) D. Wu, A. C. Sedgwick, T. Gunnlaugsson, E. U. Akkaya, J. Yoon and T. D. James, *Chem. Soc. Rev.*, 2017, **46**, 7105–

7123; (*b*) S. Erbas-Cakmak, S. Kolemen, A. C. Sedgwick, T. Gunnlaugsson, T. D. James, J. Yoon and E. U. Akkaya, *Chem. Soc. Rev.*, 2018, **47**, 2228–2248.

2 (*a*) B. Daly, J. Ling and A. P. de Silva, *Chem. Soc. Rev.*, 2015, **44**, 4203–4211; (*b*) A. P. de Silva, H. Q. N. Gunaratne, T. Gunnlaugsson, A. J. M. Huxley, C. P. McCoy, J. T. Rademacher and T. E. Rice, *Chem. Rev.*, 1997, **97**, 1515–1566; (*c*) W. Guan, W. Zhou, J. Lu and C. Lu, *Chem. Soc. Rev.*, 2015, **44**, 6981–7009; (*d*) E. B. Veale and T. Gunnlaugsson, *Annu. Rep. Prog. Chem.*, 2010, **106**, 376; (*e*) H. N. Kim, Z. Guo, W. Zhu, J. Yoon and H. Tian, *Chem. Soc. Rev.*, 2011, **40**, 79–93; Z. Guo, S. Park, J. Yoon and I. Shin, *Chem. Soc. Rev.*, 2014, **43**, 16–29.

3 (*a*) F. E. Poynton, S. A. Bright, S. Blasco, D. C. Williams, J. M. Kelly and T. Gunnlaugsson, *Chem. Soc. Rev.*, 2017, **46**, 7706–7756; (*b*) R. T. K. Kwok, C. W. T. Leung, J. W. Y. Lam and B. Z. Tang, *Chem. Soc. Rev.*, 2015, **44**, 4228–4238.

4 V. García-López, F. Chen, L. G. Nilewski, G. Duret, A. Aliyan, A. B. Kolomeisky, J. T. Robinson, G. Wang, R. Pal and J. M. Tour, *Nature*, 2017, **548**, 567–572.

5 C. Moylan, E. M. Scanlan and M. O. Senge, *Curr. Med. Chem.*, 2015, **22**, 2238–2348.

6 (*a*) S. H. Hewitta and S. J. Butler, *Chem. Commun.*, 2018, **54**, 6635–6647; (*b*) I. V. Kolesnichenko and E. V. Anslyn, *Chem. Soc. Rev.*, 2017, **46**, 2385–2390.

7 (*a*) P. A. Gale and C. Caltagirone, *Coord. Chem. Rev.*, 2018, **354**, 2–27; (*b*) A. B. Aletti, D. M. Gillen and T. Gunnlaugsson, *Coord. Chem. Rev.*, 2018, **354**, 98–120; (*c*) Z. Xu, K.-H. Baek, H. N. Kim, J. Cui, X. Qian, D. R. Spring, I. Shin and J. Yoon, *J. Am. Chem. Soc.*, 2010, **132**, 601–610.

8 (*a*) L. Fang, G. Trigiante, C. J. Kousseff, R. Crespo-Otero, M. P. Philpott and M. Watkinson, *Chem. Commun.*, 2018, **54**, 9619–9622; (*b*) X. Sun, Q. Xu, G. Kim, S. E. Flower, J. P. Lowe, J. Yoon, J. S. Fossey, X. Qian, S. D. Bull and T. D. James, *Chem. Sci.*, 2014, **5**, 3368–3373; X. Jia, Q. Chen, Y. Yang, Y. Tang, R. Wang, Y. Xu, W. Zhu and X. Qian, *J. Am. Chem. Soc.*, 2016, **138**, 10778–10781; (*c*) D. T. Shi, D. Zhou, Y. Zang, J. Li, G. R. Chen, T. D. James, X.-P. He and H. Tian, *Chem. Commun.*, 2015, **51**, 3653–3655.

9 (*a*) H. M. Burke, T. Gunnlaugsson and E. M. Scanlan, *Chem. Commun.*, 2015, **51**, 10576–10588; (*b*) Z.-R. Dai, G.-B. Ge, L. Feng, J. Ning, L.-H. Hu, Q. Jin, D.-D. Wang, X. Lv, T.-Y. Dou, J.-N. Cui and L. Yang, *J. Am. Chem. Soc.*, 2015, **137**, 14488–14495.

10 (*a*) J. I. Lovitt, C. S. Hawes, A. D. Lynes, B. Haffner, M. E. Mobius and T. Gunnlaugsson, *Inorg. Chem. Front.*, 2017, **4**, 296; (*b*) C. S. Hawes, A. D. Lynes, K. Byrne, W. Schmitt, G. Ryan, M. E. Möbius and T. Gunnlaugsson, *Chem. Commun.*, 2017, **53**, 5989–5992; (*c*) C. S. Hawes, K. Byrne, W. Schmitt and T. Gunnlaugsson, *Inorg. Chem.*, 2016, **55**, 11570–11582; (*d*) S. Mukherjee and P. Thilagar, *Chem. – Eur. J.*, 2014, **20**, 8012–8023.

11 E. Calatrava-Perez, S. A. Bright, S. Achermann, C. Moylan, M. O. Senge, E. B. Veale, D. C. Williams, T. Gunnlaugsson and E. M. Scanlan, *Chem. Commun.*, 2016, **52**, 13086–13089.

12 Examples where such targeting has been achieved: (*a*) D. Wu, S. Cheung, R. Daly, H. Burke, E. M. Scanlan and D. F. O'Shea, *Eur. J. Org. Chem.*, 2014, 6841; (*b*) Y. Fu, J. Zhang, H. Wang, J.-L. Chen, P. Zhao, G.-R. Chen and X.-P. He, *Dyes Pigm.*, 2016, **133**, 372–379; (*c*) M. H. Lee, J. H. Han, P.-S. Kwon, S. Bhuniya, J. Y. Kim, J. L. Sessler, C. Kang and J. S. Kim, *J. Am. Chem. Soc.*, 2012, **134**, 1316–1322; (*d*) R. Daly, G. Vaz, A. M. Davies, M. O. Senge and E. M. Scanlan, *Chem. – Eur. J.*, 2012, **18**, 14671–14679; (*e*) O. B. Locos, C. C. Heindl, A. Corral, M. O. Senge and E. M. Scanlan, *Eur. J. Org. Chem.*, 2010, 1026–1028.

13 (*a*) X. Jia, Y. Yang, Y. Xu and X. Qian, *Pure Appl. Chem.*, 2014, **86**, 1237–1246; (*b*) Z. Xu, L. Xu, J. Zhou, Y. Xu, W. Zhu and X. Qian, *Chem. Commun.*, 2012, **48**, 10871.

14 H.-L. Zhang, X.-Li Wei, Y. Zang, J.-Y. Cao, S. Liu, X.-P. He, Q. Chen, Y.-T. Long, J. Li, G.-R. Chen and K. Chen, *Adv. Mater.*, 2013, **25**, 4097–4101.

15 S. Cecioni, A. Imberty and S. Vidal, *Chem. Rev.*, 2015, **115**, 525–561.

16 T. J. Tymoczko, J. M. Berg and L. Stryer, *Biochemistry*, W H Freeman, 5th edn, 2002, ISBN-10: 0-7167-3051-0.

17 T. Yau, X. Dan, C. Ng and T. Ng, *Molecules*, 2015, **20**, 3791.

18 (*a*) J. M. Benito, M. Gómez-García, C. Ortiz Mellet, I. Baussanne, J. Defaye and J. M. García Fernández, *J. Am. Chem. Soc.*, 2004, **126**, 10355–10363; (*b*) V. Wittmann and R. J. Pieters, *Chem. Soc. Rev.*, 2013, **42**, 4492–4503.

19 P. N. Kanellopoulos, K. Pavlou, A. Perrakis, B. Agianian, C. E. Vorgias, C. Mavrommatis, M. Soufi, P. A. Tucker and S. J. Hamodrakas, *J. Struct. Biol.*, 1996, **116**, 345–355.

20 H. M. Burke, T. Gunnlaugsson and E. M. Scanlan, *Org. Biomol. Chem.*, 2016, **14**, 9133–9145.

21 M. Matsui and Y. Ebara, *Bioorg. Med. Chem. Lett.*, 2012, **22**, 6139–6143.

22 (*a*) R. M. Duke, E. B. Veale, F. M. Pfeffer, P. E. Kruger and T. Gunnlaugsson, *Chem. Soc. Rev.*, 2010, **39**, 3936–3953; (*b*) S. Banerjee, E. B. Veale, C. M. Phelan, S. A. Murphy, G. M. Tocci, L. J. Gillespie, D. O. Frimannsson, J. M. Kelly and T. Gunnlaugsson, *Chem. Soc. Rev.*, 2013, **42**, 1601–1618; (*c*) S. Banerjee, J. A. Kitchen, S. A. Bright, J. E. O'Brien, D. C. Williams, J. M. Kelly and T. Gunnlaugsson, *Chem. Commun.*, 2013, **49**, 8522–8524.

23 (*a*) K. Jobe, C. H. Brennan, M. Motevalli, S. M. Goldup and M. Watkinson, *Chem. Commun.*, 2011, **47**, 6036–6038; (*b*) J. Pancholi, D. J. Hodson, K. Jobe, G. A. Rutter, S. M. Goldup and M. Watkinson, *Chem. Sci.*, 2014, **5**, 3528–3535; (*c*) J. A. Kitchen, P. N. Martinho, G. G. Morgan and T. Gunnlaugsson, *Dalton Trans.*, 2014, **43**, 6468–6479; (*d*) E. B. Veale, J. A. Kitchen and T. Gunnlaugsson, *Supramol. Chem.*, 2013, **25**, 101–108; (*e*) E. Tamanini, A. Katewa, L. M. Sedger, M. H. Todd and M. Watkinson, *Inorg. Chem.*, 2009, **48**, 319; (*f*) E. Tamanini, K. Flavin, M. Motevalli, S. Piperno, L. A. Gheber, M. H. Todd and M. Watkinson, *Inorg. Chem.*, 2010, **49**, 3789; (*g*) F. Lupo, S. Gentile, F. P. Ballistreri, G. A. Tomaselli, M. E. Fragala

and A. Gulino, *Analyst*, 2010, **135**, 2273; (*h*) T. Gunnlaugsson, M. Glynn, G. M. Tocci, P. E. Kruger and F. M. Pfeffer, *Coord. Chem. Rev.*, 2006, **250**, 3094; (*i*) R. M. Duke and T. Gunnlaugsson, *Tetrahedron Lett.*, 2007, **48**, 8043; (*j*) T. Gunnlaugsson, M. Nieuwenhuyzen, L. Richard and V. Thoss, *Tetrahedron Lett.*, 2001, **42**, 4725; (*k*) T. Gunnlaugsson, B. Bichell and C. Nolan, *Tetrahedron Lett.*, 2002, **43**, 4989.

24 (*a*) E. B. Veale, D. O. Frimannsson, M. Lawler and T. Gunnlaugsson, *Org. Lett.*, 2009, **11**, 4040–4043; (*b*) E. B. Veale and T. Gunnlaugsson, *J. Org. Chem.*, 2010, **75**, 5513–5525; (*c*) S. Banerjee, S. A. Bright, J. A. Smith, J. Burgeat, M. Martinez-Calvo, D. C. Williams, J. M. Kelly and T. Gunnlaugsson, *J. Org. Chem.*, 2014, **79**, 9272–9283; (*d*) S. Murphy, S. A. Bright, F. E. Poynton, T. McCabe, J. A. Kitchen, E. B. Veale, D. C. Williams and T. Gunnlaugsson, *Org. Biomol. Chem.*, 2014, **12**, 6610–6623.

25 (*a*) S. Shanmugaraju, B. la Cour Poulsen, T. Arisa, D. Umadevi, H. L. Dalton, C. S. Hawes, S. Estalayo-Adrian, A. J. Savyasachi, G. W. Watson, D. C. Williams and T. Gunnlaugsson, *Chem. Commun.*, 2018, **54**, 4120–4123; (*b*) R. B. P. Elmes, M. Erby, S. A. Bright, D. C. Williams and T. Gunnlaugsson, *Chem. Commun.*, 2012, **48**, 2588–2590.

26 K. Hanaoka, Y. Muramatsu, Y. Urano, T. Terai and T. Nagano, *Chem. – Eur. J.*, 2010, **16**, 568–572.

27 S. Shanmugaraju, D. McAdams, F. Pancotti, C. S. Hawes, E. B. Veale, J. A. Kitchen and T. Gunnlaugsson, *Org. Biomol. Chem.*, 2017, **15**, 7321–7329.

28 *Bruker APEX-3*, Bruker-AXS Inc., Madison, WI, 2016.

29 *Bruker DIFFRAC.EVA*, Bruker-AXS Inc., Madison, WI, 2016.

30 *SADABS*, Bruker-AXS Inc., Madison, WI, 2016.

31 G. M. Sheldrick, *Acta Crystallogr., Sect. A: Found. Adv.*, 2015, **71**, 3–8.

32 G. M. Sheldrick, *Acta Crystallogr., Sect. C: Struct. Chem.*, 2015, **71**, 3–8.

33 O. V. Dolomanov, L. J. Bourhis, R. J. Gildea, J. A. K. Howard and H. Puschmann, *J. Appl. Crystallogr.*, 2009, **42**, 339–341.

